FULL PAPER

PIONEERS: a 6DoF motion sensor to measure rotation and tides in the Solar System

Valerio Filice[1,2]* , Sébastien Le Maistre[1,2], Véronique Dehant[1,2], Tim Van Hoolst[2,3], Felix Bernauer[4] and Raphaël F. Garcia[5]

Abstract

Observation of rotation variations and tides provides constraints on the interior properties of celestial bodies. Both can be precisely measured with a 6DoF (Degrees of Freedom) motion sensor placed on their surface. This type of instrument measures rotation rates and linear accelerations in a large frequency band, which includes the frequencies involved in the tides and rotation variations. A novel sensor under development aims to measure rates and accelerations with an amplitude spectral density of $2\,\mu\text{rad}\,\text{s}^{-1}\text{Hz}^{-1/2}$ and $20\,\mu\text{m}\,\text{s}^{-2}\text{Hz}^{-1/2}$ respectively in its compact version and three orders of magnitude better ($5\,\text{nrad}\,\text{s}^{-1}\text{Hz}^{-1/2}$ and $10\,\text{pm}\,\text{s}^{-2}\text{Hz}^{-1/2}$, respectively) with its high-performance version. Here, we compare these instrument performances with the precision required to measure rotation and tides in order to improve our knowledge of the interior of nine celestial bodies identified as targets for future space missions: Dimorphos, Phobos, Europa, Io, Titan, Enceladus, Triton, the Moon and Mars. Results indicate that Phobos, the Moon, and Mars cannot be investigated with the compact model, but that the interior of the other bodies can be constrained through measurements of rotation rate, and/or centrifugal acceleration, and/or tidal acceleration. We also find that the high-performance prototype instrument is suitable for acceleration measurements for all nine bodies, but not adequate for inferring interior constraints from rotation rate measurements for Triton, the Moon, and Mars. The signatures of the interior in the rotation rate and centrifugal and tidal accelerations also provide scientific requirements for future developments of 6DoF motion sensors for these nine bodies.

Keywords Rotation rate, Libration, Tidal acceleration, Interior, Solar system bodies, 6DoF sensors

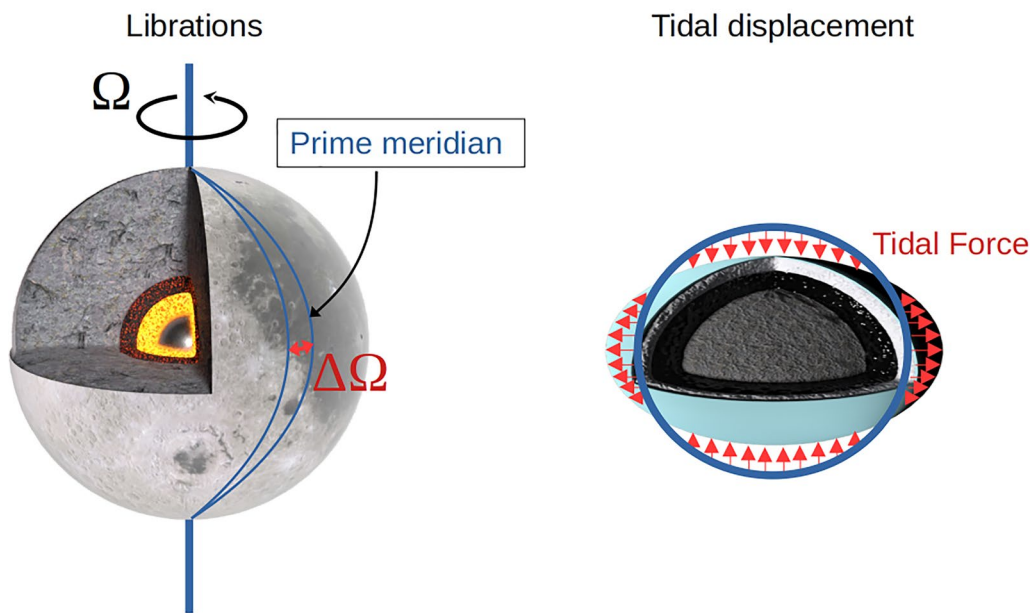*Correspondence:
Valerio Filice
v.filice@observatory.be
Full list of author information is available at the end of the article

Filice *et al. Earth, Planets and Space*   (2024) 76:12

Page 2 of 20

Graphical Abstract

6DoF motion sensor observables

Introduction

Unlike the atmosphere or surface layers, the deep interior of a celestial body cannot be directly observed. To infer information about the interior, indirect observations are used such as the body's size, mass, rotation, gravity field, magnetic field and surface deformations. In this study, we focus on the rotation changes and tidal deformations that can both be measured by a newly developed 6DoF (Degrees of Freedom) motion sensor as the one proposed by the PIONEERS project. PIONEERS, which stands for Planetary Instruments based on Optical technologies for an iNnovative European Exploration using Rotational Seismology, is a project funded by the Horizon 2020 research and innovation program of the European Commission to set the basic scientific requirements of a 6DoF motion sensor and provide an outlook of what science can be expected from the deployment of such an instrument in the Solar System.

Two different types of sensors are being developed in the PIONEERS project to address a wide range of applications: a compact model and a high-performance prototype sensor. The first consists of three orthogonally aligned quartz vibrating beam accelerometers based on Micro-Electro-Mechanical Systems (MEMS) technology and three orthogonally aligned Fiber-Optic Gyroscopes (FOGs). FOGs have significant potential to accurately measure rotational motion over a broad frequency spectrum while maintaining a high dynamic range. The operating principle of FOGs is based on the Sagnac effect, as described by Laue (1911) and Sagnac (1913), which exploits the differences in optical path lengths between two counter-propagating beams within a rotating optical fiber loop. These devices are widely used as rotation rate sensors in gyrocompasses and inertial measurement units, especially in inertial navigation (e.g. Lefèvre (1997). The PIONEERS instrument is based on a specialized FOG tailored for rotational seismology, the blueSeis-3A from iXblue (France), as presented by Bernauer (2018). The three FOG sensors measure the absolute rotation rate vector of the instrument in the 0–1000 Hz frequency range allowing to infer both the rotation rate of the planetary body and long and short-period variation of this rotation rate (Lefèvre 1997). The biases of such sensors are usually very low due to a proper temperature calibration. MEMS are commonly used for acceleration sensing in various applications, including strong-motion and engineering seismology as well as inertial navigation. These devices are characterized by their compact size, typically ranging from a few millimeters to centimeters. They integrate logic circuits and mechanical structures onto a microchip, and provide benefits such as efficient power usage, sleek design, and durability [e.g. the

Filice *et al. Earth, Planets and Space*   (2024) 76:12

Page 3 of 20

Short-Period (SP) sensors featured on the InSight mission (Lognonné et al. 2019)]. In specific, the integrated MEMS sensor is a quartz vibrating beam navigation grade accelerometer, which monitors the deformation of a vibrating beam under the influence of an acceleration (Loret et al. 2014). The use of these three MEMS sensors allows to measure the acceleration vector of the instrument in the same frequency range as the rotation rate measurements. These measurements are calibrated relative to temperature variations as well. Performance targets for the compact model include self-noise levels of $2\,\mu\mathrm{rad}\,\mathrm{s}^{-1}\mathrm{Hz}^{-1/2}$ and $20\,\mu\mathrm{m}\,\mathrm{s}^{-2}\mathrm{Hz}^{-1/2}$ within a frequency range of 0.01 Hz to 400 Hz.

The high-performance prototype integrates a Very Broadband (VBB) seismometer with an optical readout to measure translational motion, along with a giant fiber optic loop (from 0.5 m to 1 m) for rotation rate sensing. The implementation of a band-pass response with respect to acceleration enables highly sensitive broadband recording, while also mitigating problems related to saturation caused by impulsive disturbances, long-term thermal drifts, and tilt (Wielandt 2012). The VBB used in the high-performance model employs a readout devices approach based on laser interferometry principles to track the seismic mass position (see Berger et al. (2014) for a detailed comparison of different VBBs). The performance targets for this configuration are self-noise levels of $5\,\mathrm{nrad}\,\mathrm{s}^{-1}\mathrm{Hz}^{-1/2}$ and $10\,\mathrm{pm}\,\mathrm{s}^{-2}\mathrm{Hz}^{-1/2}$ across a frequency range of 0.001 Hz to 10 Hz.

The two instruments are still under development. The compact version will reach Technology Readiness Level (TRL) 5/6, while the high-performance model is being developed at TRL 3/4. To date, the FOGs of the compact models have been tested by measuring the Direct Current (DC) rotation rate of the Earth as well as high-frequency rotation rate variations induced by the vibration environment of the testing facility, showing that the instrument performs as designed. Tests of the high-performance version will be carried out in the coming year. Project's milestones and development can be followed from the project's web-page (The PIONEERS consortium 2019).

The scientific objectives of the 6DoF PIONEERS instrument threefold: (1) computing the landing trajectory of a free-falling lander; (2) determining the rotational dynamics and tidal deformation of planetary objects; and (3) measuring seismic activity from the surface of celestial bodies (Bernauer et al. 2020). In this paper we focus on the second objective, and explain and discuss in detail the ability of the PIONEERS instrument to measure the rotational and tidal motions of a celestial body. Such geodetic quantities are of paramount importance for understanding the interior properties of planetary bodies. Both tides and rotation are sensitive to the interior structure

and to the presence of internal liquid layers in particular. Separately or together, they have been used to detect and characterize a liquid core in the center of planets [e.g. Yoder et al. (2003); Le Maistre (2023) for Mars, Margot et al. (2007),Steinbrügge et al. (2018); Genova (2023) for Mercury] or subsurface oceans in icy moons [e.g. Iess (2012); Baland et al. (2011); Tajeddine et al. (2014); Thomas (2016); Van Hoolst et al. (2016)]. None of these previous discoveries relied on a 6DoF sensor though. They were mainly determined from radiometric observations or from optical data. The accuracy of the radio data is limited by the propagation noise affecting the radio waves, and both radio and optical data accuracies depend on the spacecraft trajectory accuracy when carried out from orbit. Other techniques using star trackers from the surface of bodies [e.g. Le Maistre et al. (2013)], radar speckle observations from Earth (Margot et al. 2007), or altimeter crossover measurements from orbit [e.g. Rosat et al. (2008); Mazarico et al. (2010); Stark (2015); Bertone et al. (2021)] have been used to measure tides and rotation. When possible, the performance of our PIONEERS instrument will be compared to the performances of all these alternative techniques in the present paper.

We first present the PIONEERS observables that will be used to constrain the interior of planets, namely the rotation rate, centrifugal and tidal accelerations. We then assess the contribution to these observables from the interiors of nine bodies in our Solar System that have been identified as future or potential targets for upcoming deep space missions: Dimorphos, Phobos, Europa, Io, Titan, Enceladus, Triton, the Moon and Mars. The resulting ranges of velocities and accelerations are then used to define the precision required to constrain the interior of each of these bodies using a 6DoF sensor. Finally, we discuss the results and compare the required accuracies in the determination of the bodies' rotation rate, centrifugal and tidal accelerations with the precision levels of the PIONEERS prototypes developed by iXblue and the mission requirements.

Rotation and Tide observables of a 6DoF sensor

The angular velocity vector (in a body-fixed frame) of the nine considered celestial objects is generally not uniform because of the presence of free rotational modes or because they undergo time-varying gravitational torques exerted by other solar system bodies. The way a planetary body changes its rotation and orientation in response to the external forcing is influenced by its internal structure and the dynamics of its fluid layers, if any. A fluid core or a subsurface ocean can notably change the rotation of a body since they can rotates with a different rate and around a different axis than the solid layers it interacts with [e.g. Van Hoolst et al. (2013)].

Filice *et al. Earth, Planets and Space* (2024) 76:12

Page 4 of 20

Bodies with an atmosphere like the Earth, Mars, Venus or Titan experience rotation variations resulting from angular momentum exchanges between the solid body and the atmosphere. The rotation rate variations are usually either named Length-of-Day (*LOD*) variations for atmospheric planets or longitudinal librations for bodies in spin–orbit resonance (see details on libration and ΔLOD in Van Hoolst (2015)). In the rest of the paper we will always use the word "libration" to denote periodic variations in the rotation, even for Mars where ΔLOD would be more suitable. Note that only one wave is considered in our models as, for synchronous rotators, the libration amplitude at orbital frequency is much larger than the amplitude at harmonic frequencies and is most suitable to infer interior structure properties of the body [see discussion in Le Maistre et al. (2013) for Phobos and see Van Hoolst et al. (2013) for further details]. Librations at a free libration frequency might in principle have an even larger amplitude but would require an unlikely large recent excitation. Since these amplitudes can also not reliably be predicted we do not consider them any further. Librations at frequencies of orbital perturbations can have amplitudes comparable to those of the libration at orbital frequency (see, e.g. Yseboodt et al. (2013) for the case of Mercury, Rambaux et al. (2011) for the Galilean satellites), but must be observed over much longer timescales to be estimated because of their longer periods. We here do not further consider those signals. We also restrict ourselves here to longitudinal libration and do not consider other usually smaller time-varying rotation variations such as polar motion or nutation.

The rotation rate, which is an observable of our 6DoF sensor, is expressed as a function of the libration quantities (denoted with subscripts L) as follows

$$\Omega(t) = \Omega_0 \left(1 + \frac{A_\mathrm{L} \cos\left(\Omega_L t\right)}{2\pi} \right), \tag{1}$$

where t is the time, Ω_L is the libration frequency and A_L is the libration amplitude expressed in radian, which depends on the interior properties and/or of the dynamics of the atmosphere of the body. We chose the origin of time so that the phase of libration is equal to zero. For bodies in 1:1 spin–orbit resonance such as the Moon, most of the satellites of Jupiter and Saturn and some binary asteroids, Ω_L is equal to the mean rotation frequency Ω_0, which is also equal to the orbital frequency $2\pi/T_\mathrm{orb}$ (T_orb is the orbital period).

In addition to the rotation rate, a 6DoF motion sensor can measure the centrifugal acceleration induced by the body's librations, as well as the tidal acceleration generated by the primary body (mother planet, primary asteroid or Sun). The centrifugal acceleration that will be measured by a sensor located on the surface is a

translational acceleration whose amplitude depends on the latitude ϕ of the sensor as

$$a_c(t) = \Omega(t)^2 r \cos(\phi), \tag{2}$$

where r is the distance from the center of the body.

The tidal acceleration a_T that will be measured by the 6DoF motion sensor is the combination of the direct tidal acceleration at the surface a_dT, the tidal displacement of the ground described by the Love number h, and the effect of the mass redistribution due to the tides related to Love number k (Love 2015) according to $a_T = a_\mathrm{dT}\left(1 + h - \frac{3}{2}k\right)$. The direct tidal acceleration can be estimated evaluating the perturbations on the body's potential due to tides and the total tidal acceleration can be expressed as

$$a_T(t) = \delta \frac{GM_p r}{d(t)^3} \Gamma, \tag{3}$$

where $\delta = 1 + h - \frac{3}{2}k$ is the so-called tidal gravimeter factor, $\Gamma = 6e$ for synchronous bodies or $\Gamma = \frac{3}{2}$ for fast rotators, e and d are the eccentricity and the distance to center of mass of the perturbing body. Because d varies over time, we determine the average amplitude of the tidal signal by calculating the mean distance of the body w.r.t. the primary. A detailed derivation of Eq. (3) is given in Appendix A.

Equations 1–3 describe the observables of the PIONEERS motion sensor. Because we are interested in the bodies' interior properties, which affect the libration amplitude A_L in Eqs. (1, 2), we rewrite the observables as the difference between the measured rate and acceleration and those of a body rotating at the constant rate Ω_0:

$$\Omega_\mathrm{lib} = \Omega_0 \left(\frac{A_\mathrm{L} \cos\left(\Omega_L t\right)}{2\pi} \right), \tag{4}$$

$$a_{c_\mathrm{lib}} = \Omega_0^2 \left(\frac{A_\mathrm{L} \cos(\Omega_L t)}{2\pi} \right)^2 r \cos(\phi). \tag{5}$$

Following the same procedure, we could have rewritten the tidal observable as $a_T - a_\mathrm{dT}$, given the fact that the dependence to the interior of the tidal acceleration is carried by the Love numbers (h, k). However, this does not give any added value and we prefer to use δ as the parameters of interest to infer the interior from tidal accelerations. We thus keep Eq. (3) to model that observable.

As explained in "Introduction" section, both the PIONEERS models feature three FOG sensors that measure rotation rate variations and three MEMS sensors that measure linear and centrifugal accelerations and their short-period variations as those induced by seismic events or by the interactions between the lander and the

Filice *et al. Earth, Planets and Space*   (2024) 76:12

Page 5 of 20

ground. Consequently, the two instruments are able to perform independent measurements of the rotation and the acceleration vectors.

Interior signatures

The science requirements for the instruments design are defined based on the physical signal one wants to detect. In our case, such a signal corresponds to the signature of the interior in the body's rotation rate and centrifugal acceleration as well as in the tidal acceleration. In this section, we propose a method to determine the precision of the PIONEERS observables needed to improve our knowledge of the interior of a given body. This corresponds to the measurement precision needed to distinguish between different interior model predictions. For that, we must measure with an error significantly smaller than the signal itself and than the difference between two end member predictions. Model predictions are based on Eqs. (3–5) and the ranges of interior signature in the observables are obtained by substituting the expected amplitude of libration in Eqs. (4, 5) and that of the expected tidal gravimeter factor in Eq. (3) by the minimum $(A_{L_{\min}}, \delta_{\min})$ and maximum $(A_{L_{\max}}, \delta_{\max})$ values allowed by interior models. The precision needed for the observables shall thus be smaller than $(A_{L_{\max}} - A_{L_{\min}})\partial(Rot)/\partial(A_L)$ for the rotation observables with $Rot \in \{\Omega_{lib}; a_{c_{lib}}\}$, and smaller than $(\delta_{\max} - \delta_{\min})\partial g_{dT}/\partial \delta$ for the tidal observable. Consequently, the needed precision in the rotation rate measurement can be defined as

$$p_\Omega = \kappa \Omega_0 \left(\frac{A_{L_{\max}} - A_{L_{\min}}}{2\pi} \right), \tag{6}$$

that of the centrifugal acceleration measurement as

$$p_{a_c} = \kappa \Omega_0^2 \left(\frac{A_{L_{\max}} - A_{L_{\min}}}{\pi} \right) r \cos(\phi), \tag{7}$$

and that of the tidal acceleration measurements as

$$p_{a_T} = \kappa (\delta_{\max} - \delta_{\min}) \frac{GM_p r}{d^3} \Gamma, \tag{8}$$

where d is the average distance to the perturbing body and κ is a scale factor to be set within]0; 1[given the level of precision wanted.

The geophysical signal in the PIONEERS observables could be hidden by errors in other quantities defining them, namely Ω_0, Ω_L, r and ϕ for the rotation and of G, M_p, r, Γ and d for the tides (see Eqs. 3, 4 and 5). The time tag errors, which affect all types of data, must also be maintained (by design) smaller than the interior signal. For the real data analysis, all these errors will have to be taken into account when inferring interior properties

from the observables. A per-body rough estimation of these levels and a short discussion about them is provided in Appendix B.

As explained, the PIONEERS instrument is a combination of a FOG, a MEMS and a VBB whose performances are expressed in the frequency domain. Therefore, the above precisions shall be expressed in this domain if we want to compare them to the sensor self-noise level or translate them into requirements for the instruments of future missions. The Amplitude Spectral Density (ASD) of a pure sine wave of amplitude S, as those involved in our rotational and tidal observables, can be calculated as a function of the total observation duration (or mission duration) defined as $t_m = n * T_{orb}$ (with $n \in \mathbb{N}$)

$$S_{ASD} = S\sqrt{t_m/2}. \tag{9}$$

The interested reader may refer to Appendix C for a full derivation.

Physical and dynamical parameters of the selected bodies

The nine bodies considered in this study have been identified by the scientific community and space agencies as targets for future missions. Besides the five ones considered in Bernauer et al. (2020), namely Dimorphos, Phobos, Europa, The Moon and Mars, we also consider here Io, Titan, Enceladus and Triton for the reasons explained below.

An orbiter mission to Io was proposed for the NASA Discovery program, but was not selected (McEwen et al. 2019). Nevertheless, Io will be studied through a couple of flybys of Juno in 2024 (Hansen et al. 2022) and will most likely be the target of a future mission, as the least known Galilean moon in the Jovian system, after the JUICE and Europa clipper missions are completed. Measurement of Io's tides and rotation variations are key since one can use them to characterize the melt zone and confirm or nor the presence of a global magma ocean beneath the surface (Bierson and Nimmo 2016; Van Hoolst et al. 2020). Identified as ocean worlds from Cassini's tides and rotation measurements (Iess 2012; Thomas 2016), both Titan and Enceladus are attractive bodies that will be visited again in a near future. The NASA Dragonfly lander mission, planned for arrival at Titan in the mid-2030 s (Barnes 2021), is a good candidate to host our compact sensor, as is the lander of the proposed Enceladus Orbilander NASA flagship mission, which will be dedicated to search for chemicals conducive to life in the ocean of Enceladus (MacKenzie 2021). Triton as well has always attracted interest from the scientific community as evidenced by the multiple mission proposed after the only

Filice *et al. Earth, Planets and Space*   (2024) 76:12

Page 6 of 20

close encounter made by Voyager 2 in 1989. Neptune Odyssey is the last mission proposed by NASA to the Neptune–Triton system (Rymer 2021). It includes an orbiter and an atmospheric probe. Odyssey has unfortunately been recently abandoned in favor of a mission to the Uranian system, but this is only a postponement since studying Neptune, its rings, moons and space environment as well as Triton is of primary importance (National Academies of Sciences, Engineering, and Medicine 2022).

We describe here the selected physical and dynamical parameters of the aforementioned bodies that we used for the calculation of the expected rotation and tidal signals and their amplitude levels. Most of these values are taken from the literature and they are gathered in Table 1. For Dimorphos and Triton, the values are evaluated and discussed here below.

The asteroid binary system Didymos–Dimorphos is the target of the NASA Double Asteroid Redirection Test (DART) mission. DART is the first demonstration of the kinetic impactor technique in the framework of Planetary Defense techniques (Rivkin and Cheng 2023). Physical characteristics of Dimorphos have been estimated by Daly (2023) using the DRACO camera on board the spacecraft. Post-impact orbital characteristics are described by Thomas (2023). The librations remained unassessed during the DART mission; however, the forthcoming ESA's Hera mission (Michel 2022) holds the promise of filling this knowledge gap. We therefore rely on the latest predictions of the rotation dynamics. The libration angle of Dimorphos is highly dependent on changes to its velocity, and therefore Dimorphos has a different libration state after the DART impact (Richardson 2022). The libration of the secondary is expected to be close to zero pre-impact and up to a maximum of 7° for the post-impact nominal case. However, from the parametric study realized by Richardson (2022) to overcome the multiple unknowns of the secondary dynamics and shape, as well as the impact effects, four resonance frequencies have been determined that can be reached by a multitude of combination of semi-axis ratios leading to a chaotic motion or attitude instability. For the majority of semi-axis ratios combinations such as $a/b \geq 1.3$, the maximum libration angle in longitude is about 45°. We therefore choose a libration amplitude A_L range from 6° to 45° taking out the resonance cases since a conservative instrument design will not jeopardize its functioning for higher magnitudes of the measured signal (Fig. 1).

Given that tides affecting the Didymos system are currently poorly constrained, we compute the tidal Love numbers assuming a deformable, homogeneous and incompressible spherical body according to Love (2015)

$$h = \frac{5}{3}k = \frac{5}{2}\left(1 + \frac{19}{2}\frac{\mu}{g\rho r}\right)^{-1}, \tag{10}$$

where ρ is the bulk density of the body, g the surface gravity, r the mean radius and μ the rigidity of the rocks that compose it. Since it is believed that Dimorphos could be a rubble-pile body, we use $\tilde{\mu}_r \gtrsim \sqrt{\mu/\epsilon_Y}$ to compute its rigidity Goldreich and Sari (2009). According to the nominal values of the system as assumed by Daly (2023), we set $\rho = 2400 \pm 300$ kg m^{-3} and $r = 75.5 \pm 1.25$ m. Following Naidu (2020), the Young's modulus E is fixed at 10^7 Pa, the Poisson's ratio ν equal to 0.25 and the yield strain ϵ_Y equal to 10^{-2}. We calculate the shear modulus μ from the equation of isotropic materials resulting in $\tilde{\mu}_r \approx \sqrt{E/((2(1+\nu))\epsilon_Y)} \approx 6$ kPa and therefore $h \in [2.86 - 4.25] \times 10^{-4}$ and $k \in [1.72 - 2.55] \times 10^{-4}$.

It will be much more challenging to probe the interior of Triton from the measurement of its rotation and tides because both are expected to be very small due to its orbital eccentricity close to zero ($e \sim 10^{-5}$, Jacobson (2009)). The libration amplitude A_L of Triton can be expressed as (Duxbury and Callahan 1981):

$$A_L = \frac{2e}{1 - \frac{1}{3\gamma}}, \tag{11}$$

where $\gamma = (B - A)/C$ and $(A < B < C)$ are the principal moments of inertia. Actual knowledge of Triton's shape is not accurate enough to constrain its moment of inertia (Thomas 2000). We calculate the relative difference between moments of inertia from the secular Love number k_s (a measure of the body-yield to centrifugal deformation in the course of its secular evolution) using Eq. 20 from Comstock and Bills (2003):

$$\gamma = \frac{45k_s q}{18 + 25k_s q}. \tag{12}$$

$q = M_p/M_b(r/a)^3$ is a dimensionless quantity where M_p is the mass of Neptune, M_b and r are the mass and the radius of Triton, respectively, and a is the orbit's semi-major axis. Differently from Comstock and Bills (2003), who took the hydrostatic value $k_s = 3/2$, we consider a range of values in agreement with values of other icy satellites with which Triton shares most of its physical characteristics, i.e. $k_s \in [0.9 - 1.5]$ (McKinnon and Kirk 2014). The resulting range of A_L is $[3.2°, 5.4°] \times 10^{-6}$ (i.e. only at milliarcsecond level) showing that the variations of Triton's rotation rate and acceleration are very small (see Table 1). The signatures of the internal structure are then expected to be even smaller, unless the presence of a subsurface ocean would strongly increase the amplitude (Van Hoolst et al. 2013). To calculate Triton's tides, we calculate a set of interior structure models of Triton that

Filice *et al. Earth, Planets and Space*   (2024) 76:12

Page 7 of 20

Table 1 Physical and dynamical parameters of the selected bodies

Body	r (km)	Mass (kg)	Parent body mass (10^{24} kg)	Mean orbital distance d (km)	T_{orb} (day)	Ω_0 [rad s^{-1}]	$\dot{\Omega}_0$ [rad s^{-2}]	A_L [°]		Tidal acceleration (ms^{-2})	k_2	h_2	
Dimorphos	75.5×10^{-3}	4.84×10^{9}	Didymos: 5.557×10^{-13}	1.20	0.474	1.46×10^{-4}	2.14×10^{-8}	[7.00,45.00]	This study	1.694×10^{-6}	$[1.72,2.55] \times 10^{-4}$	$[2.86,4.25] \times 10^{-4}$	This study
Phobos	11.08	1.06×10^{16}	Mars: 0.642	9.40×10^{3}	0.319	2.28×10^{-4}	5.20×10^{-8}	[1.08,1.10]	Lainey (2021)	5.710×10^{-4}	$[0.53,5.30] \times 10^{-4}$	$[0.88,8.80] \times 10^{-4}$	Le Maistre et al. (2013)
Europa	1560.80	4.80×10^{22}	Jupiter: 1898.125	6.71×10^{5}	3.551	4.92×10^{-4}	2.42×10^{-7}	$[2.42,3.80] \times 10^{-2}$	Van Hoolst et al. (2013)	1.226×10^{-3}	[1.20,1.30]	$[2.3,2.7] \times 10^{-1}$	Van Hoolst et al. (2013)
Io	1821.49	8.93×10^{22}	-"-	4.22×10^{5}	1.769	4.11×10^{-5}	1.69×10^{-9}	$[0.53,3.12] \times 10^{-1}$	Van Hoolst et al. (2020)	6.129×10^{-3}	$[5.1,8.3] \times 10^{-2}$	[0.09,2.1]	Van Hoolst et al. (2020)
Titan	2574.73	1.35×10^{23}	Saturn: 568.317	1.22×10^{6}	15.945	1.10×10^{-4}	1.20×10^{-8}	$[4.19,7.69] \times 10^{-3}$	Van Hoolst et al. (2013)	8.922×10^{-5}	$[5.49,6.83] \times 10^{-1}$	[1.30,1.70]	Iess (2012), Durante et al. (2019)
Enceladus	252.10	1.08×10^{20}	–	2.38×10^{5}	1.372	5.30×10^{-5}	2.81×10^{-9}	$[1.05,1.35] \times 10^{-1}$	Thomas (2016)	7.774×10^{-4}	$[1.00,7.00] \times 10^{-2}$	$[0.15,1.9] \times 10^{-1}$	Van Hoolst et al. (2016), Baland et al. (2016)
Triton	1352.60	2.14×10^{22}	Neptune: 102.409	3.55×10^{5}	5.877	1.24×10^{-5}	1.53×10^{-1}	$[3.2,5.4] \times 10^{-6}$	This study	2.870×10^{-4}	$[0.1,3.4] \times 10^{-1}$	[0.1,1.2]	This study
Moon	1737.40	7.346×10^{22}	Earth: 5.972	3.84×10^{5}	27.322	2.66×10^{-6}	7.08×10^{-12}	$[4.66,4.67] \times 10^{-3}$	Rambaux and Williams (2010)	1.223×10^{-5}	$[2.22,2.26] \times 10^{-2}$	$[3.64,3.78] \times 10^{-2}$	Konopliv (2013), Lemoine (2013)
Mars	3389.50	6.417×10^{24}	Sun: 1988500	1.52 au	686.97	7.09×10^{-5}	5.02×10^{-9}	$[1.22,3.25] \times 10^{-6}$	Konopliv et al. (2020)	2.805×10^{-8}	$[1.66,1.82] \times 10^{-1}$	$[3.08,3.38] \times 10^{-1}$	Konopliv et al. (2020)

References for Dimorphos are Daly (2023) and Thomas (2023)

All other radii are taken from Archinal et al. (2018)

Masses and orbital parameters values are from the Jet Propulsion Laboratory—Solar System Dynamics website

For the Moon, we consider the Lunar Laser Ranging (LLR) uncertainty on the libration as the signature of the interior signal to retrieve

For Mars, we consider the uncertainties in the *LOD* variations at the orbital period (annual terms) as the level of precision to reach in order to further constrain the Mars rotation variations and thereby the planet's atmospheric cycles

The h_2 values have been estimated from several Mars interior models such that they match the range of the measured k_2 values (A. Rivoldini personal communication)

satisfy the observed mass and radius. Similarly to other outer Solar System satellites, we assume that Triton has a metallic core, a silicate mantle and an icy shell, with a possible subsurface ocean. We further assume that the interior is hydrostatic (follows the fluid pressure–depth relation). By solving the equation describing the deformation of a self-gravitating, spherically symmetric body (Alterman et al. 1959; Sabadini and Vermeersen 2004), we calculate the Love number h_2 and k_2 and we predict $h_2 \in [0.15 - 1.2]$ and $k_2 \in [0.1 - 0.32]$. We assumed that the ice shell, ocean, mantle and core have a uniform density and that they are incompressible.

Predicted signals levels and required precision

For each body considered in this paper, we computed the interior-related ranges of rotation rates and centrifugal and tidal accelerations using the physical and dynamical parameters provided in Table 1. The difference between the minimum and the maximum values of each range is shown in Fig. 2. It corresponds to the level of the signature of the bodies' interior in the observables. Libration and tidal periods are considered to be equal to the bodies' orbital period, T_{orb}. The centrifugal accelerations are evaluated at the equator (i.e. with $\phi = 0$ in Eq. 2). As per the order of magnitude of the differences in the rotation rate, three bodies stand out: Triton, the Moon and Mars. These are very challenging targets for a 6DoF sensor since the low eccentricity of Triton leads to a small rotation rate and a small centrifugal acceleration, whereas the rotation rates of Mars and the Moon are already precisely measured. Figure 2 also shows the predicted contribution of the interiors to tidal accelerations. Two bodies can be distinguished by their tidal signal, which is much greater than the others for Io and much smaller than the

others for Dimorphos. The former is due to the fact that we account for the effect of a subsurface magma ocean in the calculation of the tidal gravimeter factor (δ) of Io. For Dimorphos, the signal is extremely small due its small size and to the small mass of Didymos. It is worth noting that the ranges computed for the outer system bodies are rough estimates since only limited data are available for most of them (see references in Table 1). For all bodies in spin–orbit resonance, we considered the tides related to their non-zero orbital eccentricity. These eccentricity tides are larger than the obliquity tides, which are due to the moon's axial tilt relative to its orbital plane (see Tyler (2009)), except for Triton, which has a very small eccentricity of 1.6×10^{-5} but a significantly large obliquity of up to 0.7° Chen et al. (2014). As a consequence, Triton's obliquity tides are three times larger than its eccentricity tides. However, since the required measurement precision is the one that allows distinguishing between different interior model predictions, and because both types of tidal accelerations linearly depend on the gravimeter factor (see Eqs. 8 and 17 of Appendix A), the instrument requirement is roughly the same for both obliquity and eccentricity tidal accelerations.

Given the signal shown in Fig. 2, we have computed the precisions needed to infer information about the bodies' interior. Tables 2 and 3 show the results that have been obtained by setting $\kappa = 0.1$ in Eqs. (6–8), to measure the signals with a precision one order of magnitude better than the difference between the minimum and maximum contributions from the interior.

Assuming a mission duration t_m 10 times longer than the orbital period of the body, we then compute the ASD of these targeted precisions using Eq. 9 to convert them into instrument requirements. For Mars, we set a mission

Table 2 Required measurement precisions in the rotation rate and acceleration along with the associated 6DoF instrument requirements corresponding to the ASD of these precisions

Body	Libration frequency (Hz)	p_Ω [rads^{-1}]	$p_{\Omega_{ASD}}$ [rad/s/$\sqrt{\mathrm{Hz}}$]	p_{a_c} [ms^{-2}]	$p_{a_{c_{ASD}}}$ [m/s^2/$\sqrt{\mathrm{Hz}}$]	Mission duration (days)
Dimorphos	2.330×10^{-5}	1.55×10^{-6}	7.16×10^{-4}	3.71×10^{-8}	1.72×10^{-5}	5
Phobos	3.628×10^{-5}	1.27×10^{-9}	4.70×10^{-7}	6.40×10^{-9}	2.38×10^{-6}	3
Europa	3.259×10^{-6}	7.87×10^{-11}	9.75×10^{-8}	5.03×10^{-9}	6.23×10^{-6}	35.5
Io	6.542×10^{-6}	2.97×10^{-9}	2.59×10^{-6}	4.44×10^{-7}	3.88×10^{-4}	17.5
Titan	7.259×10^{-7}	4.43×10^{-12}	1.16×10^{-8}	1.04×10^{-10}	2.72×10^{-7}	160
Enceladus	8.436×10^{-6}	4.42×10^{-10}	3.40×10^{-7}	1.18×10^{-8}	9.09×10^{-6}	14
Triton	1.969×10^{-6}	7.40×10^{-15}	1.18×10^{-11}	2.47×10^{-13}	3.95×10^{-10}	60
Moon	4.209×10^{-7}	1.11×10^{-14}	3.80×10^{-11}	1.02×10^{-13}	3.51×10^{-10}	275
Mars	1.128×10^{-5}	4.00×10^{-14}	6.89×10^{-10}	1.92×10^{-11}	3.31×10^{-8}	687

The mission duration used to compute the requirements (i.e. ASD quantities) corresponds to 10 times the orbital period except for Mars for which we set to be equal to one martian year

Filice *et al. Earth, Planets and Space*   (2024) 76:12

Page 9 of 20

Table 3 Required measurement precisions in the tidal acceleration along with the associated 6DoF instrument requirements corresponding to the ASD of these precision

Body	Tidal frequency (Hz)	p_{a_T} (ms^{-2})	$p_{a_{T_{ASD}}}$ (m/s^2/$\sqrt{\text{Hz}}$)	Mission duration (days)
Dimorphos	2.330×10^{-5}	2.82×10^{-13}	1.31×10^{-10}	5
Phobos	3.628×10^{-5}	3.96×10^{-10}	1.47×10^{-7}	3
Europa	3.259×10^{-6}	1.41×10^{-7}	1.75×10^{-4}	35
Io	6.542×10^{-6}	1.45×10^{-5}	1.27×10^{-2}	18
Titan	7.258×10^{-7}	1.87×10^{-7}	4.90×10^{-4}	160
Enceladus	8.435×10^{-6}	1.62×10^{-7}	1.25×10^{-4}	14
Triton	1.969×10^{-6}	1.20×10^{-9}	1.91×10^{-6}	60
Moon	4.236×10^{-7}	3.21×10^{-10}	1.10×10^{-6}	275
Mars	1.685×10^{-8}	3.31×10^{-11}	3.59×10^{-7}	687

The mission duration used to compute the requirements (i.e. ASD quantities) corresponds to 10 times the tidal period except for Mars for which we set to be equal to one martian year

duration equal to one orbital period (i.e. one martian year) to keep reasonable mission duration. In Figs. 3, 4, 5, these instrument requirements (also reported in Tables 2 and 3) are superimposed with the self-noise levels of the PIONEERS instrument, which are defined for $f > 0.001\ Hz$ (Bernauer et al. 2020):

- Rotation rate measurements: $2\ \mu\text{rad/S}/\sqrt{\text{Hz}}$ for the compact version and $5\ \text{nrad/S}/\sqrt{\text{Hz}}$ for the high-performance prototype,
- Translational (centrifugal and tidal) acceleration measurements: $20\ \mu\text{m/s}^2/\sqrt{\text{Hz}}$ for the compact version and $10\ \text{pm/s}^2/\sqrt{\text{Hz}}$ for the high-performance prototype.

We assume that these noise levels are constant below 0.001 Hz, i.e. for libration and tidal frequencies (see Tables 2 and 3). In fact, thermal variations will introduce a noise at the same frequencies as libration and tides, with amplitudes depending on the environment and on the system in which the sensor is integrated. However, we neglect such thermal noise because it will most probably be shifted in phase with respect to the target signals and can be calibrated using a model derived from ground measurements.

Under the above assumptions (i.e. $\kappa = 0.1$, $t_m = 10 * T_{\text{orb}}$ and the noise levels), one can conclude that the compact version of the 6DoF sensor would only be suitable for measuring the rotation rate of Dimorphos and Io (Fig. 3), while the high-performance (HP) version of the instrument would be good enough to make use of rotation rate measurements also for Phobos, Europa,

Titan and Enceladus. For Triton, Mars and the Moon, an even high-performance sensor would be needed to measure the rotation rate with enough precision to gain information about their interior. In Fig. 4, one can see that the HP version would allow to constrain the interior of the nine bodies by measuring the centrifugal acceleration on their surface and that the compact version would still be suitable for a mission to Io. (For Europa and Io in particular, the radiation environment might place enormous challenges on mission and sensors. We assume here that our sensor will be well-protected from such aggressive radiations.) Similarly, tidal accelerations (Fig. 5) can be measured with the HP sensor with sufficient accuracy for all selected bodies while the less precise compact model would not meet the required accuracy for Dimorphos, Phobos, Triton, the Moon and Mars. It is finally interesting to note that combining the three observables allows the compact version of the PIONEERS instrument to constrain the interior properties of all the bodies considered in this study except Phobos, Triton, the Moon and Mars. Moreover, such a combined analysis would certainly be very powerful to infer the bodies' interior due to the complementarity of these observables (see Van Hoolst et al. (2020) for an example of this complementarity for Io).

The labels (framed numbers) in Figs. 3–5 indicate the target accuracies of the libration amplitudes, expressed in degrees, and that of the tidal gravimetric factors enabling direct comparison with other instrument performances published in recent literature. In particular, we compare with the performances predicted for the Radio-Science (RS) experiment of the Europa Clipper mission (Mazarico et al. 2023), those of a multidisciplinary experiment on board the Hera mission to the Didymos system (Michel 2022), and those of an experiment combining RS and star-tracker measurements collected from the surface of Phobos (Le Maistre et al. 2013). The Europa Clipper RS experiment foresees a determination of the libration amplitude with ~400 m (i.e. 0.015°) uncertainty, and a determination of the tidal Love numbers k_2 and h_2 with uncertainties of 0.014 and 0.1, respectively (Mazarico et al. 2023), which translates into an uncertainty of 0.12 on δ. The former is 10 times larger than the precision needed (~ 40 m), and that we can reach with both PIONEERS models as shown in Fig. 3, to constrain Europa's interior from libration. The latter is 2 orders of magnitude higher than the 0.004 target precision for δ, easily achievable with PIONEERS. We note that an RS experiment on an orbiter mission will be more precise than a multi-flyby mission as Europa Clipper. The ESA JUICE mission (Grasset 2013), which will be inserted in orbit around in Ganymede in 2034, is expected to measure k_2 of Ganymede at the level of 10^{-4} (Cappuccio 2020) and

to reach a measurement accuracy of on h_2 of a few percent (Steinbrügge et al. 2015). Assuming a typical value of h_2 of 1.3 and an accuracy of 2%, we determine an uncertainty in δ at 10^{-2}. If we use this value as an order of magnitude of the expected precision of tidal measurements from a spacecraft orbiting an icy moon, we find that it will only outperform the target precision of Io by 1 order of magnitude. The Dimorphos libration will be estimated by Hera with a 0.02° precision (Gramigna et al. 2023) by combining direct-to-Earth RS data with Inter-Satellite radio links, optical data and altimetric data. This is 2 orders of magnitude better than what we can get from the PIONEERS compact model, but 3 orders of magnitude higher compared to the rotation rate measurement precision reachable with PIONEERS HP model alone (i.e. without using other instruments). No prediction for the measurement of tides by Hera has been published so far. Finally, the Japanese Martian Moons eXploration (MMX) mission will be put in orbit around Phobos in a couple of years and should determine the Phobos libration amplitude with a 0.02° accuracy (Matsumoto et al. 2021). This is 10 times larger than our target accuracy. RS from a lander would meet the required precision for the libration estimate, but would still be unable to measure tides with sufficient precision (Le Maistre et al. 2013). At Phobos, the PIONEERS compact/HP model would measure in about 3 days the libration amplitude at the $2 \times 10^{-3°}$ level and the tides with 7×10^{-6} precision, while RS and star-tracker would provide libration with 0.001° uncertainty and tides with 0.001 uncertainty after a couple of weeks of operation (Le Maistre et al. 2013), showing the great interest of the PIONEERS instrument.

Mission duration is a key parameter in defining instrument performance. To properly measure periodic signals, the best is to get observations over a duration t_m larger than one entire period T of the target signal, i.e. $t_m = nT$ with $n > 1$. This is why we computed the ASD of the required precisions assuming the nominal mission duration to be 10 times the period of the rotational and tidal motions. For the sake of inter-body comparison, we kept $n = 10$ for each quantity reported in Tables 2 and 3 and in Figs. 3, 4, 5, except for Mars for which we set $n = 1$ to avoid an unrealistically long mission ($\sim$20 years). This setting leads to quite stringent duration for a mission at Titan (160 days), at Triton (60 days) or at the Moon (275 days). However, one could think of reducing these missions life time (with $1 < n < 10$) given the margin offered by the instrument performances (i.e. the difference between PIONEERS's self-noise (horizontal lines) and body-dependent required accuracy (black circles) in Figs. 3–5). Indeed, because the needed accuracy, when expressed in ASD, depends on the mission duration according to $\sqrt{t_m/2}$, one can easily identify the best

suited t_m that would make the mission as short as possible while guaranteeing the scientific objectives. Figure 6 shows how much varies the required instrument precision as a function of the number n of orbital periods covered by the mission with respect to the nominal case of $n = 10$. For instance, if the mission life time is reduced to its minimum (i.e. $n = 1$), then the precision to achieve is $\sim$70% smaller than if we were taking measurements over 10 periods ($n = 10$) as considered above. This approach reduces instrument-related challenges and significantly eases lifetime-related constraints in mission design. However, it comes at the cost of only being able to observe for a single orbital period. Generally speaking, Fig. 6 shows us that the longer is the mission relatively to the orbital period of the celestial body, the more demanding is the instrument precision needed to probe the interior of a celestial object (note that the three observables will be affected the same way by the mission duration since t_m appears only in the ASD conversion factor). There is a balance between the instrument performance and the mission duration that we can tune to optimize the mission scenario given by the margin of the body-dependent required accuracy w.r.t. the instrument self noise as explained above. For instance in the case of the Moon, the usage of the HP sensor permits to reduce the mission duration to one orbital period since it would measure tidal accelerations with the required precision already after 27 days. Similarly, one could reduce the problematic duration of a mission to Titan or Triton down to one orbital period (i.e. 16 days and 6 days, respectively), and still get information about their interior from tides' measurements using the compact sensor or the HP sensor. For Titan, it is also possible to use the HP sensor measuring rotation rate if the mission duration is at least twice the orbital period. For Io, instead, six orbital period is the minimum if we want to infer interior proprieties from rotation rate measurements using the compact model. In Table 4, one can see the minimum number of orbital periods (i.e. minimum mission duration) necessary to gain knowledge about the bodies' interior depending on the PIONEERS model used.

Conclusions

A 6DoF sensor has recently been proposed to improve the science return of future planetary missions by accurately measuring centrifugal and tidal accelerations and rotation rate experienced by a spacecraft landed on a celestial body (Bernauer et al. 2020). Such an instrument is currently being developed by the iXblue French company within the PIONEERS framework, an Horizon 2020 research and innovation program of the European Commission. The instrument consists in a combination of Fiber-Optic Gyroscopes (FOGs),

Table 4 Minimum number of orbital periods (n_{min}) required to reach the targeted accuracy ($\kappa = 0.1$) for the three observables, depending on the PIONEERS model (compact versus high-performance)

Body	n_{min} (Compact)			n_{min} (HP)		
Observables	Ω	a_c	a_T	Ω	a_c	a_T
Dimorphos	1	Ø	Ø	1	1	1
Phobos	Ø	Ø	Ø	1	1	1
Europa	Ø	Ø	1	1	Ø	1
Io	6	Ø	1	1	1	1
Titan	Ø	Ø	1	2	Ø	1
Enceladus	Ø	Ø	1	1	1	1
Triton	Ø	Ø	1	Ø	Ø	1
Moon	Ø	Ø	Ø	Ø	Ø	1
Mars	Ø	Ø	Ø	Ø	Ø	1

n_{min} is related to the mission duration by $t_{m_{min}} = n_{min} T_{orb}$

micro-electro-mechanical systems (MEMS) and a very-broad-band seismometer (VBB), which makes it perfectly well-suited to measure the rotation, tides and quakes of a celestial object.

The present study provides details regarding the determination of the rotation and tides of the five bodies considered by Bernauer et al. (2020), namely Dimorphos, Phobos, Europa, the Moon and Mars, along with four additional bodies also identified as probable target for future missions: Io, Titan, Enceladus and Triton. For all these bodies, the level of precision in the rotation rate and centrifugal and tidal accelerations necessary to improve our knowledge of their interior structure (or atmosphere dynamics for Mars) has been identified and converted into requirements for a 6DoF sensor. We then discussed the relevance of deploying a 6DoF sensor on each of these nine objects, by comparing the required measurement accuracy and the targeted self-noise of the PIONEERS instrument. The former depends on the mission duration because it has to be expressed in Amplitude Spectral Density (ASD) to be compared to the latter. Following Bernauer et al. (2020), two levels of self-noise for the instrument have been considered: that of a compact instrument capable of measuring linear acceleration spectral density at a level of 10^{-5} m/s^2/$\sqrt{Hz}$ and rotation rate spectral density at 10^{-6} rad/s/$\sqrt{Hz}$, and that of a high-performance instrument about one thousand times more accurate (10 pm s^{-2}Hz$^{-1/2}$ and 5 nrad s^{-1}Hz$^{-1/2}$, for linear acceleration and rotation rate, respectively). Assuming for each body a mission operating over 10 orbital periods (except for Mars for which we set to be equal to only one martian year), we found that Phobos, the Moon and Mars could not be investigated with the PIONEERS compact model, while the others could all

have their interior constrained from either the measurement of their rotation rate and/or centrifugal acceleration and/or tidal acceleration with such a model. We also found that the PIONEERS high-performance prototype instrument would be suitable for all nine bodies with regard to the acceleration measurements, but would still not be good enough to infer interior constraints from rotation rate measurements in the case of Triton, the Moon and Mars. Furthermore, the precision of PIONEERS' instruments is comparable or superior to the RS experiments of upcoming Phobos and Europa missions. Precise measurements of Phobos' libration amplitude such as those provided by PIONEERS, coupled with more precise measurements of the degree-two gravity field from the upcoming MMX mission, can confirm the heterogeneous interior of the Martian moon, as explained by Le Maistre et al. (2019). Accurate tidal measurements of Europa will help to determine the thickness and rheology of the ice shell, as well as the density of the ocean. This information is crucial for assessing the Jovian moon's potential for habitability (Mazarico et al. 2023). These examples demonstrate the relevance of libration and tidal measurements in advancing our understanding of the origins of our Solar System and the identification of potentially habitable environments within our Solar System, making this instrument worthy of consideration in a payload suite for a future mission. We finally pointed out the balance existing between the instrument performance and the mission duration: the longer the mission is, the more accurate is the instrument precision needed. Given this, we have identified for each body the shortest mission duration allowed by the instrument self-noise that would still achieve the geophysical objectives considered in this paper.

Table 5 $\Delta = 1\sigma$ Uncertainties in bodies' mass and radius from Jet Propulsion Laboratory—Solar System Dynamics website

Body	$\Delta r [km]$	$\Delta M_p [10^{24} kg]$
Dimorphos	0.004	Didymos: 5e−15
Phobos	0.04	Mars: 0.000030
Europa	0.30	Jupiter: 0.088
Io	0.50	–
Titan	0.02	Saturn: 0.026
Enceladus	0.20	–
Triton	2.40	Neptune: 0.0048
Moon	0.1	Earth: 0.00028
Mars	0.2	Sun: 7e-11

Values of the Didymos system are from Daly (2023)

Appendix A: Total tidal acceleration

An accelerometer on the surface can measure the direct tidal acceleration as well as the induced accelerations due to the displacement of the surface resulting from the mass redistribution inside the body. We provide here the detailed derivation of Eq. 3.

The tidal potential (V_t) perturbs the body gravity potential (V). Manipulating the tidal potential equation truncated at degree two, the variations in the external potential field can be expressed as

$$\left| \frac{V_T}{V} \right| \approx \frac{M_p}{M_b}\left(\frac{r}{d} \right)^3 \Gamma, \tag{13}$$

where M_p is the mass of the perturbing body, d is the distance between the center of mass of the two bodies, r is the radius of the body and Γ is equal to $6e$ for synchronous bodies or $3/2$ for fast rotators. The ratio between the direct tidal (a_{dT}) and self-gravitational ($g = GM_b/r^2$) accelerations equals the corresponding ratio between tidal (V_T) and gravitational potentials V; therefore, using Eq. 3, we can write

$$\frac{a_{dT}}{g} = \frac{V_T}{V} = \frac{M_p}{M_b}\left(\frac{r}{d} \right)^3 \Gamma, \tag{14}$$

from where the expression of a_{dT} can easily derived. The acceleration as measured by a system on the surface of the body feels the direct tidal attraction a_{dT}, the displacement of the surface related to the Love number h (hV_T/g) and the effect of the mass redistribution due to the tides related to Love number k (additional potential at surface kV_T). The combination $\delta = 1 + h - k$ defines the tidal gravimeter factor that is used to express the total tidal acceleration

$$a_T = \delta a_{dT} = \delta \frac{GM_p r}{d^3} \Gamma. \tag{15}$$

Since d is time-dependent, to evaluate the average amplitude of the tidal signal we use the mean distance of the body with respect to the primary.

If the moon's spin axis is tilted relative to its orbital plane, a second tidal force is due to the moon's obliquity. The tidal potential due to obliquity tides is defined by Eq. 2 in (Tyler 2009) and it is proportional to

$$V_{T_o} \propto \frac{3}{2}\Omega^2 r^2 I, \tag{16}$$

where Ω is the rotation rate and I the obliquity. Using the same reasoning as above, we can express the total tidal acceleration due to obliquity as

$$a_{T_o} = \delta a_{dT_o} \propto \delta \frac{3}{2}\Omega^2 r I. \tag{17}$$

Appendix B: Sensitivity analysis and levels of precision

Here, we quantify the sensitivity of the PIONEERS observables to the different parameters defining them and compare that of the target-interior parameters (i.e.

Table 6 Relative contributions to PIONEERS observables

Body	$\Delta A_L/A_L$	$\Delta\Omega_0/\Omega_0$	$\Delta r/r$	$\Delta M_p/M_p$	$\Delta d/d$	$6\Delta e/e$	$\Delta\delta/\delta$
Dimorphos	1.4	0.048	5.298	0.07	0.1	∼0	1.38e−5
Phobos	0.018	0.008	0.361	4.7e−7	0.004	0.452	7.65e−7
Europa	0.44	1e−5	0.019	6.6e−6	0.002	0.923	0.02
Io	2.00	4e−4	0.027	6.6e−6	0.007	2.610	0.98
Titan	0.6	2e−5	0.001	1.9e−6	0.0005	0.042	0.11
Enceladus	0.25	3e−4	0.079	1.9e−6	0.002	0.252	0.0078
Triton	0.6	0.14	0.177	1.4e−4	0.009	0.1	0.43
Moon	0.003	∼0	0.006	2e−7	∼0	∼0	8.0e−4
Mars	1.00	∼0	0.006	7.5e−9	∼0	∼0	7.9e−3

Filice *et al. Earth, Planets and Space*   (2024) 76:12

Page 13 of 20

Table 7 Required data timing accuracy to measure libration amplitudes

Body	Δt [s]
Dimorphos	4.775e−2
Phobos	9.154e−4
Europa	1.992e−3
Io	1.799e−2
Titan	6.238e−4
Enceladus	2.900e−3
Triton	1.629e−3
Moon	1.866e−6
Mars	1.551e−2

A_L and δ) with that of the uncertainties/errors in all the other parameters entering in Eqs. (3–5). The relative contribution of each parameter to the PIONEERS observables are given below at first order in the Δ quantities:

$$\frac{\Delta\Omega}{\Omega} \approx \frac{\Delta A_\mathrm{L}}{A_\mathrm{L}} + \frac{\Delta\Omega_0}{\Omega_0} - t^2\Omega_L\Delta\Omega_L - \Omega_L^2 t\Delta t, \quad (18)$$

$$\frac{\Delta a_c}{a_c} \approx \frac{2\Delta A_\mathrm{L}}{A_\mathrm{L}} + \frac{2\Delta\Omega_0}{\Omega_0} - 2t^2\Omega_L\Delta\Omega_L \\ - 2\Omega_L^2 t\Delta t + \frac{\Delta r}{r} - \tan(\phi)\Delta\phi, \quad (19)$$

$$\frac{\Delta a_T}{a_T} \approx \frac{\Delta\delta}{\delta} + \frac{\Delta M_p}{M_p} + \frac{\Delta r}{r} - \frac{3\Delta d}{d} + \frac{\Delta\Gamma}{\Gamma}. \quad (20)$$

To evaluate each term of the above equation, we use numerical values reported in Table 1 for M_p and reference radii r, and the numerical values of their associated variations are taken from Table 5, assuming $\Delta = 1\sigma$ of the considered parameter.

Except for Mars, all the bodies considered in this study are in 1:1 spin–orbit resonance, so we have $\Omega_0 = \Omega_L = 2\pi/T_\mathrm{orb} = l$, with l the mean motion. $\Gamma = 3/2$ for fast rotators like Mars, but it becomes variable for synchronous bodies for which $\Gamma = 6e$ and $\Delta\Gamma/\Gamma = 6\Delta e/e$. Therefore, Ω_0, Γ and d are all related to the orbit of the bodies. We thus infer the order of magnitude of $\Delta\Omega_0$, Δd and Δe for each body from the accuracy of their orbit, which is taken from literature and/or quantified here by comparing two recent ephemeris, one from the IMCCE team and the other from JPL, when both are available. Figure 8 shows $\Delta d/d$, Δl and $\Delta e/e$ for each body. For Triton, there are no ephemeris from IMCCE, so we use the same error as Io for d

(i.e. $\Delta d \sim 30\,km$) and conservative errors of 0.01% for its rotation rate and of 0.1% for its orbital eccentricity. Table 6 provides per observable and in percent, the relative contributions/errors of each quantity affecting the PIONEERS measurements. Uncertainties in the lander position are usually very small. Figure 8 shows how an error in the lander latitude propagates to the centrifugal acceleration. We see that for low-latitude landers, positional errors are negligible and that an error lower than 0.001° in the lander latitude should be targeted for high-latitude landers. Note that we considered equatorial landers in the paper, so position error has no influence on a_c in our study. The reference radius, r, is the limiting factor which can surpass the target signal if the topography of the body is poorly known. In particular, current knowledge on Dimorphos shape could prevent us from properly retrieve the libration amplitude from centrifugal acceleration and the tidal gravimeter factor from the tidal acceleration. Nevertheless, the periodic signature of the libration signal in a_c could still be detectable and if not, then one could still determine librations from the rotation rate observable, which is not depending on r. The same reasoning applies to Phobos and the Moon, for which the signature of Δr in a_c is slightly larger than the signature of the interior in the libration amplitudes (see Tab. 6). Note that for Dimorphos, the large uncertainty in r will be reduced by the forthcoming Hera mission. The determination of the tidal gravimeter factor, δ, is the most challenging. It only exceeds the noise coming from the uncertainties in the other parameters for Europa, Io, Titan, Triton and Mars.

An error in the data timing can also hide the target signal. To avoid this, we need the onboard computer to time tag the PIONEERS observations with a precision that induces relative errors smaller than $\Delta A_\mathrm{L}/A_\mathrm{L}$ and smaller than $\Delta\delta/\delta$. As timing errors multiplied by t in the expressions for the total error on the rotation rate and centrifugal acceleration (see Eq. 18–20), we compute Δt when maximum, i.e. at $t = t_m = nT_\mathrm{orb}$ with $n = 10$ (except for Mars where n is set to 1 as done in the rest of the calculations of the paper), such that

$$\Delta t < \frac{1}{20\pi\,\Omega_L}\frac{\Delta A_\mathrm{L}}{A_\mathrm{L}}, \quad (21)$$

and $\Delta t_{Mars} = 10\Delta t$ for the rotation rate observable. For centrifugal acceleration the time tag requirements reported in Table 7 must be divided by 2. For tidal acceleration measurements, the timing error is of the order of that of $\Delta d/d$.
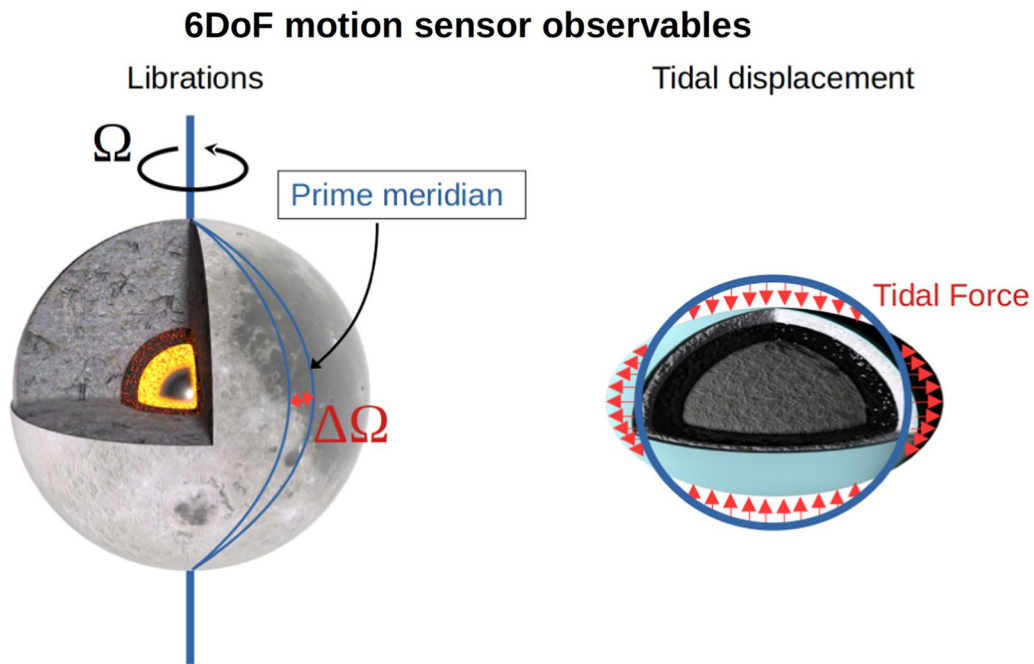
Fig. 1 Schematic representation of the observables that can be measured with the 6DoF motion sensor developed by the PIONEERS programme, namely rotation variations (left panel) and tidal deformation (right panel). These types of observations are excellent tools for inferring the interior structure of Solar System bodies, represented here by Mars (left panel) and a possible interior structure of icy moons with a subsurface ocean beneath an icy crust (right panel). The bodies shown are not to scale
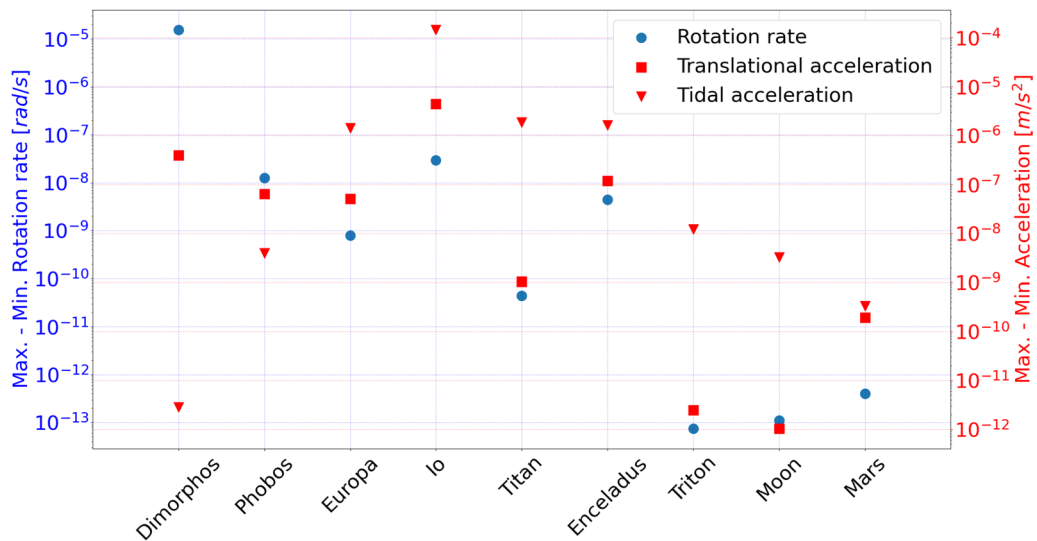
Fig. 2 Difference between the maximum and minimum of the expected signal levels according to possible interior structure models. The centrifugal acceleration is evaluated at the equator ($\phi = 0$), with the values of the radii shown in Table 1
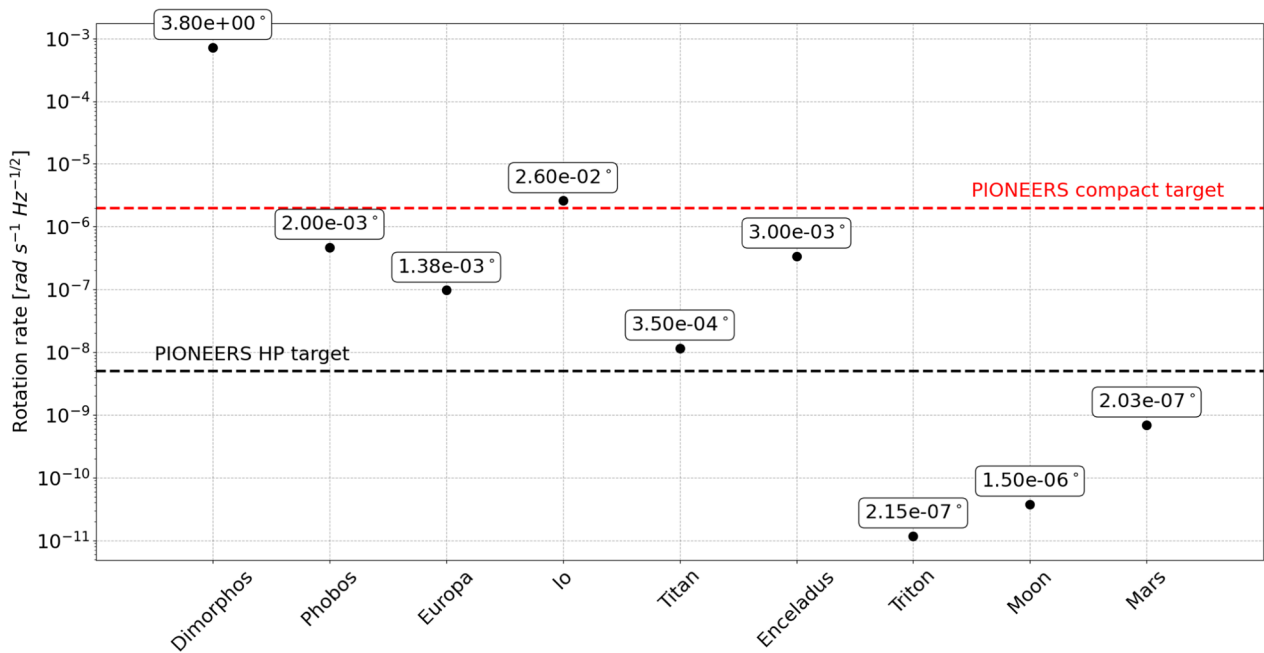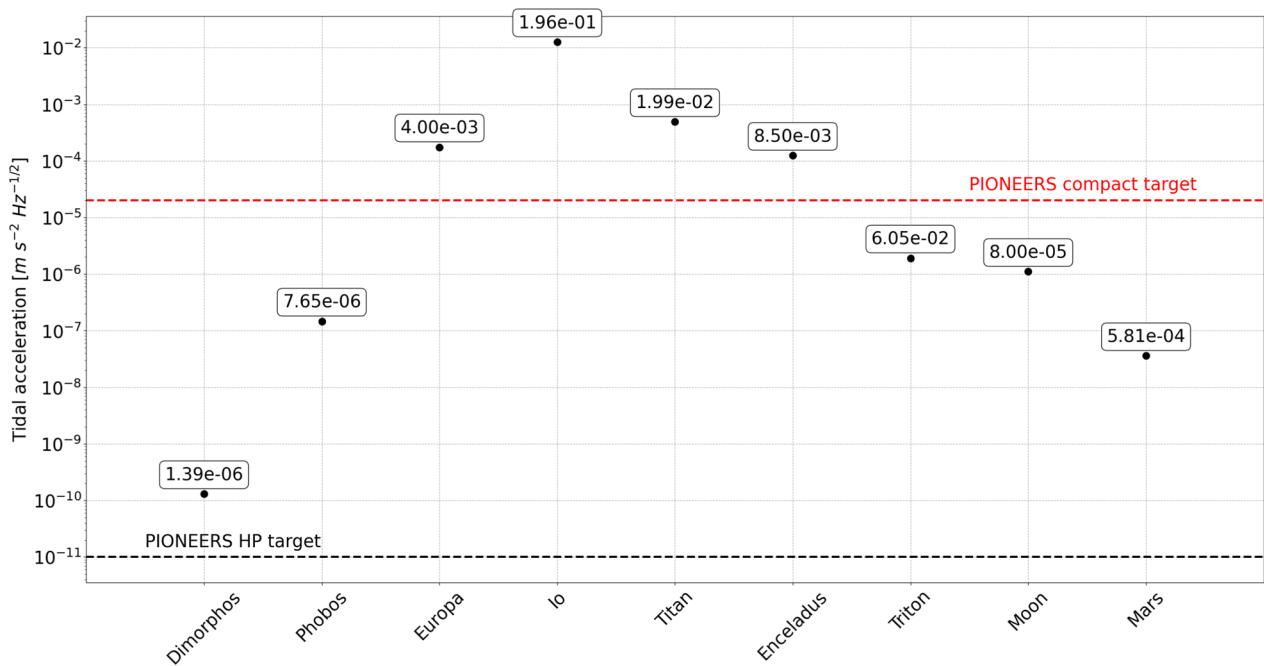
Fig. 3 Required precision in rotation rate measurements for the nine selected bodies assuming a mission duration of 10 times the libration periods specific for each body, except Mars whereby the mission duration is equal to one Martian year. The dashed red and black lines are, respectively, the compact and high-performance foreseen precision of the instruments, i.e. the instrument self-noise. The labels show the aimed libration amplitude accuracies for the instrument's measurements. The values are in degrees and are equal to $\kappa[A_{L_{max}} - A_{L_{min}}]$ with $\kappa = 0.1$
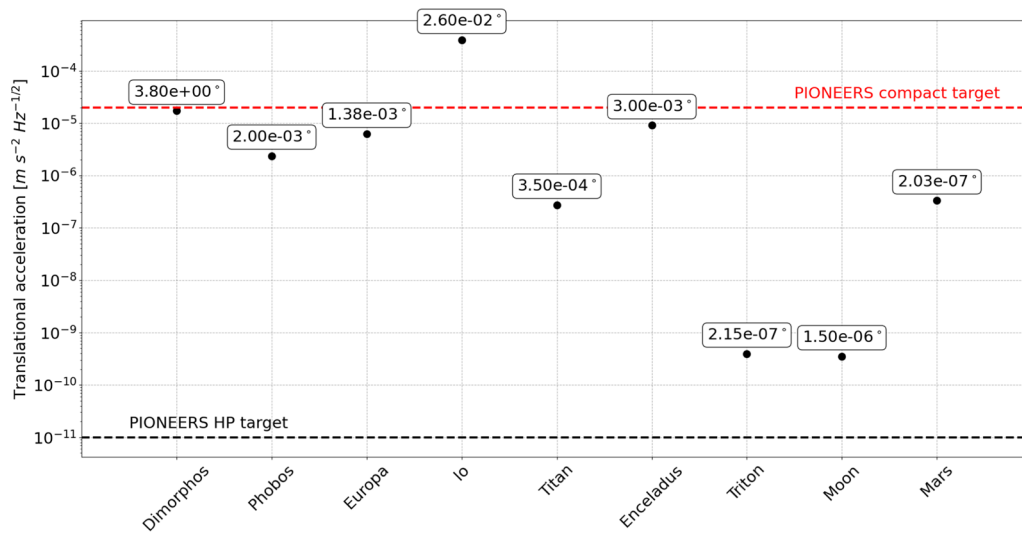
Fig. 4 Required precision in centrifugal acceleration measurements for the nine selected bodies assuming a mission duration of 10 times the libration periods specific for each body, except Mars whereby the mission duration is equal to one Martian year. The accelerations are evaluated at the equator ($\phi = 0$), with the values of the radii shown in Table 1. The dashed red and black lines are, respectively, the compact and high-performance foreseen precision of the instruments, i.e. the instrument self-noise. The labels show the aimed libration amplitude accuracies for the instrument's measurements. The values are in degrees and are equal to $\kappa[A_{L_{max}} - A_{L_{min}}]$ with $\kappa = 0.1$

Fig. 5 Required precision in tidal acceleration measurements for the nine selected bodies assuming a mission duration of 10 times the tidal periods specific for each body, except Mars whereby the mission duration is equal to one Martian year. The dashed red and black lines are, respectively, the compact and high-performance foreseen precision of the instruments, i.e. the instrument self-noise. The labels show the aimed tidal gravimeter factor accuracies for the instrument's measurements. The values are equal to $\kappa[\delta_{max} - \delta_{min}]$ with $\kappa = 0.1$
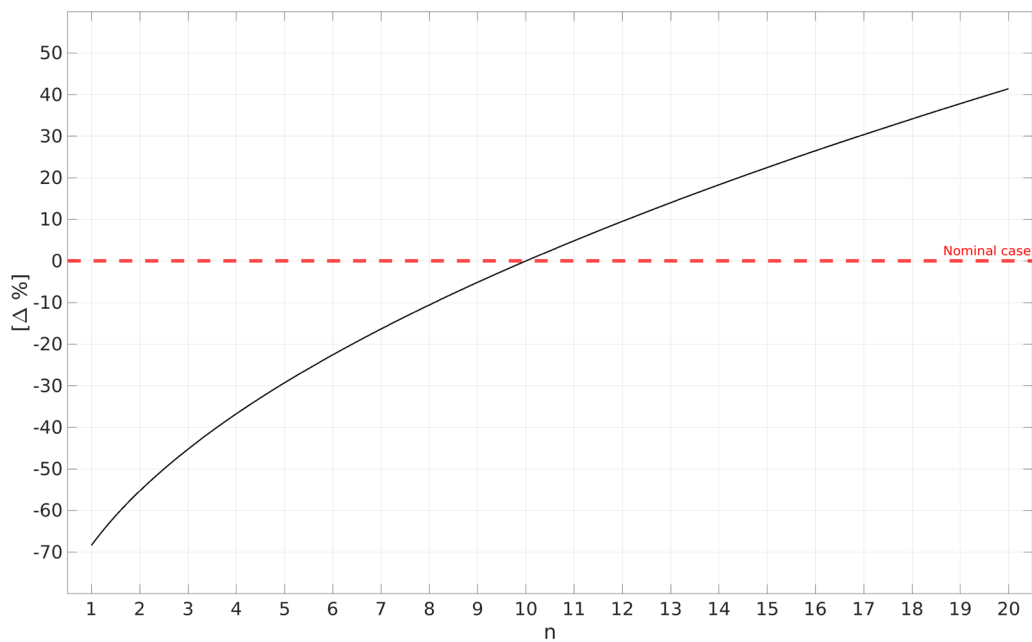
Fig. 6 Relative percentage difference of the required precision as a function of the number n of orbital periods during which observations are taken. The variation of the required precision is expressed relatively to the nominal case obtained with $n = 10$. The number of periods defines the mission duration as $t_m = nT_{orb}$, which is used in the ASD conversion factor $\sqrt{t_m/2}$ that is equal for every observables
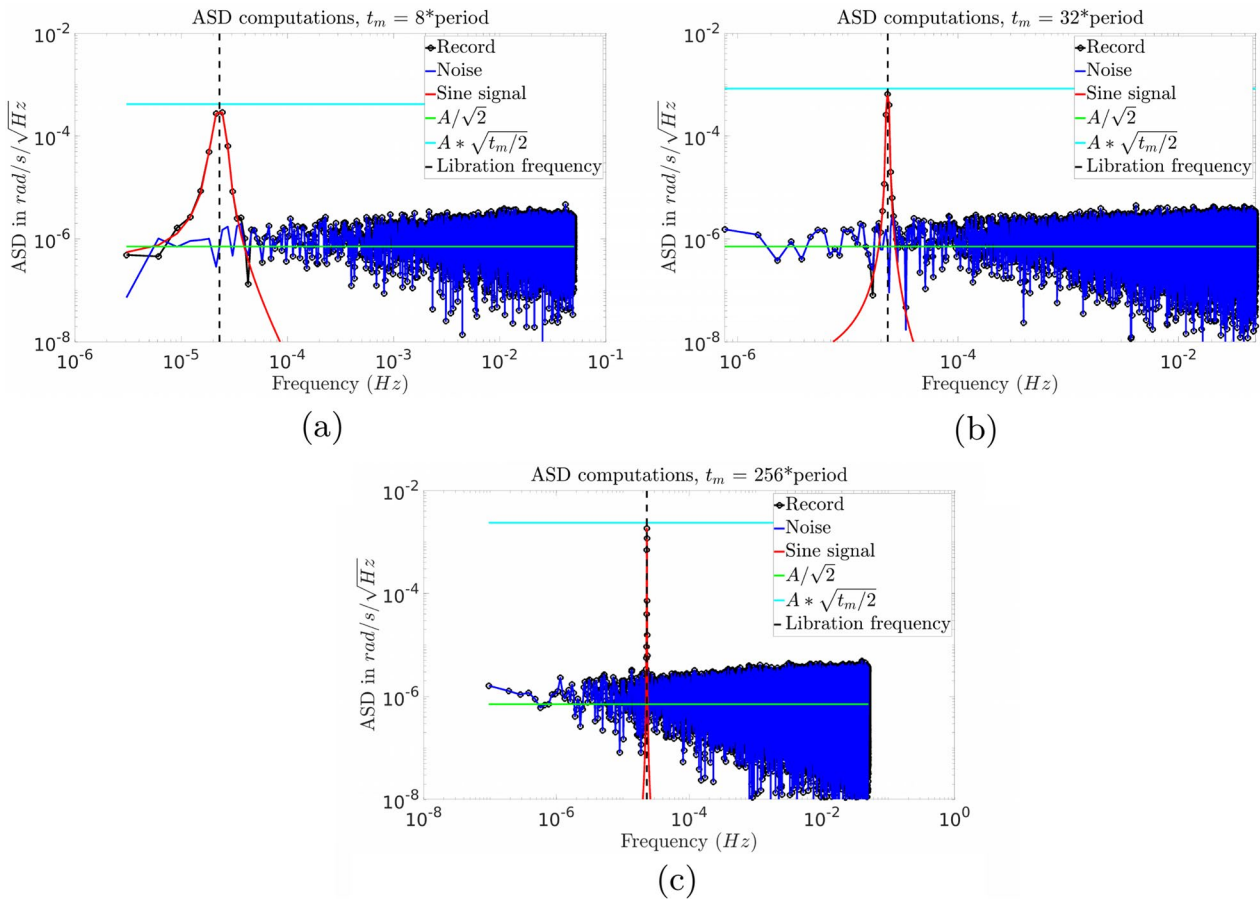
Fig. 7 Numerical calculation of the ASD of a pure sine with white noise for different observation duration of 8 (**a**), 32 (**b**) and 256 (**c**) times the target signal period. The traditional approximation (green line) fails to predict the ASD value, while Eq. (23) (cyan line) successfully provides the effective amplitude of the signal

Appendix C. Amplitude Spectral Density (ASD) of a pure sine signal

The calculation of the ASD of a pure sine wave is represented in the frequency domain as a single peak at its own frequency, with an amplitude proportional to the strength of the wave. The ASD level of a pure sine wave depends on the associated frequency and bandwidth. Using the approach defined by Bormann and Wielandt (2013) for signals with a finite bandwidth, we know that the root mean square (RMS) amplitude (or effective amplitude) of a wavelet f(t) can be approximated as (Eq.4.16 in Bormann and Wielandt (2013))

$$A_{\text{RMS}} = S = \sqrt{P \times (f_u - f_l)}, \tag{22}$$

where P is the power spectral density, and f_u and f_l are the upper and lower corner frequencies of the bandpassed signal. Assuming a signal with a 1/3 octave bandwidth centered around the frequency f_0, we have $(f_u - f_l) = 0.23 f_0$. Given the fact that $f_0 = 1/T$, where T is the period of the signal, and the total observation duration defined as $t_m = 10T$, we can write

$$S_{\text{ASD}} = \sqrt{P} = A_{\text{RMS}}\sqrt{\frac{t_m}{2.3}} \approx S\sqrt{\frac{t_m}{2}}. \tag{23}$$

This formula differs from the classical approximation ($S/\sqrt{2}$), by the fact that it relies on the observation duration (t_m), i.e. on the frequency and bandwidth of the signal. Figure 7 shows that our Eq. (23) correctly approximates the effective amplitude of a sinusoidal signal while the classical approximation ($S/\sqrt{2}$) does not.
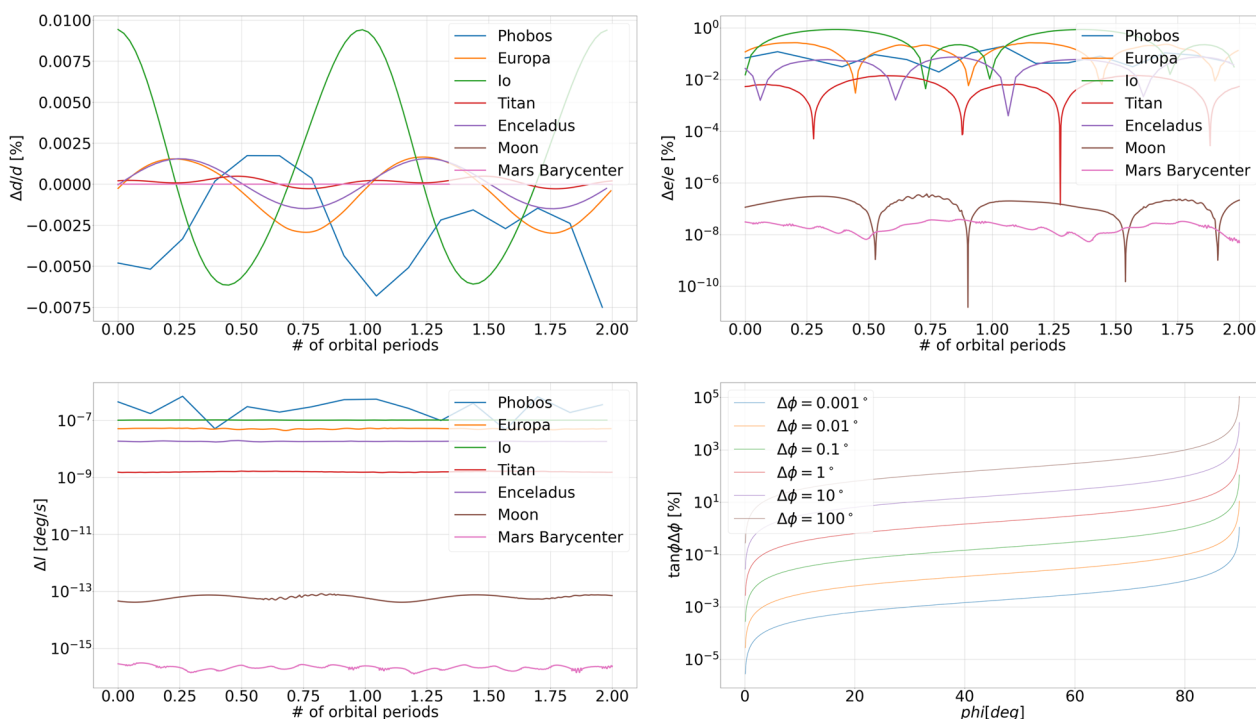
Filice *et al. Earth, Planets and Space*   (2024) 76:12

Page 18 of 20

Fig. 8 Relative errors in parameters *d* and *e* (top panels) and absolute errors in mean anomaly, *l* (bottom-left panels) for each body. Bottom-right shows the relative signature in a_c induced by a given error in the lander latitude, $\Delta\phi$

Author contributions
Methodology: VF, VD, SLM, TVH. Formal analysis: VF, VD, SLM, TVH. Writing—original draft: VF, VD, SLM, TVH. Writing—review and editing: SLM, TVH, FB, RG. Oversight and leadership responsibility: FB, RG. Project administration: VD, RG.

Availability of data and materials
The datasets used and/or analyzed during the current study are available from the corresponding author on reasonable request.

Declarations

Competing interests
The authors declare that they have no competing interests.

Author details
[1]Earth and Life Institute, Université catholique de Louvain, Place Louis Pasteur 3, 1348 Louvain-la-Neuve, Belgium. [2]Reference Systems and Planetology, Royal Observatory of Belgium, 3 Avenue Circulaire, 1180 Uccle, Belgium. [3]Instituut voor Sterrenkunde, Katholieke Universiteit Leuven, Celestijnenlaan 200d, 3001 Leuven, Belgium. [4]Department für Geo und Umweltwissenschaften, Ludwig-Maximilians Universität MÜnchen, Theresienstrasse 41, 80333 München, Germany. [5]Institut Supérieur de l'Aéronautique et de l'Espace, 10 Avenue Edouard Belin, 31055 Toulouse, France.

References
Alterman Z, Jarosch H, Pekeris CL, Jeffreys H (1959) Oscillations of the earth. Proc R Soc London Ser Math Phys Sci 252(1268):80–95. https://doi.org/10.1098/rspa.1959.0138

Archinal BA et al (2018) Report of the IAU working group on cartographic coordinates and rotational elements: 2015. Celest Mech Dyn Astron. https://doi.org/10.1007/s10569-017-9805-5

Baland R-M, Hoolst TV, Yseboodt M, Karatekin O (2011) Titan's obliquity as evidence of a subsurface ocean? Astron Astrophys 530:A141. https://doi.org/10.1051/0004-6361/201116578

Baland R-M, Yseboodt M, Van Hoolst T (2016) The obliquity of Enceladus. Icarus 268:12–31. https://doi.org/10.1016/j.icarus.2015.11.039

Barnes JW et al (2021) Science goals and objectives for the Dragonfly Titan rotorcraft relocatable lander. Planet Sci J 2(4):130. https://doi.org/10.3847/psj/abfdcf

Berger J, Davis P, Widmer-Schnidrig R, Zumberge M (2014) Performance of an optical seismometer from 1 hz to 10 hz. Bull Seismol Soc Am 104(5):2422–2429. https://doi.org/10.1785/0120140052

Bernauer F et al (2018) BlueSeis3a: full characterization of a 3c broadband rotational seismometer. Seismol Res Lett 89(2A):620–629. https://doi.org/10.1785/0220170143

Bernauer F et al (2020) Exploring planets and asteroids with 6DoF sensors: Utopia and realism. Earth Planets Space. https://doi.org/10.1186/s40623-020-01333-9

Bertone S, Mazarico E, Barker MK, Goossens S, Sabaka TJ, Neumann GA, Smith DE (2021) Deriving mercury geodetic parameters with altimetric crossovers from the mercury laser altimeter (MLA). J Geophys Res Planets. https://doi.org/10.1029/2020je006683

Bierson CJ, Nimmo F (2016) A test for Io's magma ocean: modeling tidal dissipation with a partially molten mantle. J Geophys Res Planets 121(11):2211–2224. https://doi.org/10.1002/2016je005005

Bormann P, Wielandt E (2013) Seismic signals and noise, chapter 4. Geo-ForschungsZentrum GFZ, Potsdam

Cappuccio P et al (2020) Ganymede's gravity, tides and rotational state from JUICE's 3gm experiment simulation. Planet Space Sci 187:104902. https://doi.org/10.1016/j.pss.2020.104902

Chen E, Nimmo F, Glatzmaier G (2014) Tidal heating in icy satellite oceans. Icarus 229:11–30. https://doi.org/10.1016/j.icarus.2013.10.024

Comstock RL, Bills BG (2003) A solar system survey of forced librations in longitude. J Geophys Res. https://doi.org/10.1029/2003JE002100

Daly RT et al (2023) Successful kinetic impact into an asteroid for planetary defence. Nature 616(7957):443–447. https://doi.org/10.1038/s41586-023-05810-5

Durante D, Hemingway D, Racioppa P, Iess L, Stevenson D (2019) Titan's gravity field and interior structure after Cassini. Icarus 326:123–132. https://doi.org/10.1016/j.icarus.2019.03.003

Duxbury TC, Callahan JD (1981) Pole and prime meridian expressions for Phobos and Deimos. Astron J 86:1722. https://doi.org/10.1086/113056

Genova A et al (2023) Regional variations of mercury's crustal density and porosity from MESSENGER gravity data. Icarus 391:115332. https://doi.org/10.1016/j.icarus.2022.115332

Goldreich P, Sari R (2009) Tidal evolution of rubble piles. Astrophys J 691(1):54–60. https://doi.org/10.1088/0004-637x/691/1/54

Gramigna E et al (2023) The hera radio science experiment at didymos. Astrophysics. https://doi.org/10.48550/arXiv.2310.11883

Grasset O et al (2013) JUpiter ICy moons explorer (JUICE): an ESA mission to orbit Ganymede and to characterise the Jupiter system. Planet Space Sci 78:1–21. https://doi.org/10.1016/j.pss.2012.12.002

Hansen CJ et al (2022) Juno's close encounter with ganymede—an overview. Geophys Res Lett. https://doi.org/10.1029/2022gl099285

Iess L et al (2012) The tides of Titan. Science 337(6093):457–459. https://doi.org/10.1126/science.1219631

Jacobson RA (2009) The orbits of the neptunian satellites and the orientation of the pole of Neptune. The Astron J 137(5):4322–4329. https://doi.org/10.1088/0004-6256/137/5/4322

Konopliv AS et al (2013) The JPL lunar gravity field to spherical harmonic degree 660 from the GRAIL primary mission. J Geophys Res Planets 118(7):1415–1434. https://doi.org/10.1002/jgre.20097

Konopliv AS et al (2020) Detection of the chandler wobble of mars from orbiting spacecraft. Geophys Res Lett. https://doi.org/10.1029/2020gl090568

Lainey V et al (2021) Mars moon ephemerides after 14 years of mars express data. Astron Astrophys 650:A64. https://doi.org/10.1051/0004-6361/202039406

Laue M (1911) Üer einen versuch zur optik der bewegten körper. Münchener Sitzungsberichte 663:405–412

Le Maistre S et al (2023) Spin state and deep interior structure of mars from InSight radio tracking. Nature 619(7971):733–737. https://doi.org/10.1038/s41586-023-06150-0

Le Maistre S, Rosenblatt P, Rambaux N, Castillo-Rogez JC, Dehant V, Marty J-C (2013) Phobos interior from librations determination using Doppler and star tracker measurements. Planet Space Sci 85:106–122. https://doi.org/10.1016/j.pss.2013.06.015

Le Maistre S, Rivoldini A, Rosenblatt P (2019) Signature of phobos' interior structure in its gravity field and libration. Icarus 321:272–290. https://doi.org/10.1016/j.icarus.2018.11.022

Lefèvre HC (1997) Fundamentals of the interferometric fiber-optic gyroscope. Opt Rev. https://doi.org/10.1007/bf02935984

Lemoine FG (2013) High-degree gravity models from GRAIL primary mission data. J Geophys Res Planets 118(8):1676–1698. https://doi.org/10.1002/jgre.20118

Lognonné P et al (2019) SEIS: insight's seismic experiment for internal structure of mars. Space Sci Rev. https://doi.org/10.1007/s11214-018-0574-6

Loret T et al (2014) Navigation grade accelerometer with quartz vibrating beam. In: Loret T (ed) 2014 DGON inertial sensors and systems (ISS). IEEE, Karlsruhe

Love AE H (2015) Some Problems of Geodynamics. University of Cambridge ESOL examinations

MacKenzie SM et al (2021) The Enceladus Orbilander mission concept: balancing return and resources in the search for life. Planet Sci J 2(2):77. https://doi.org/10.3847/psj/abe4da

Margot JL, Peale SJ, Jurgens RF, Slade MA, Holin IV (2007) Large longitude libration of mercury reveals a molten core. Science 316(5825):710–714. https://doi.org/10.1126/science.1140514

Matsumoto K et al (2021) MMX geodesy investigations: science requirements and observation strategy. Earth Planets Space. https://doi.org/10.1186/s40623-021-01500-6

Mazarico E et al (2023) The europa clipper gravity and radio science investigation. Space Sci Rev. https://doi.org/10.1007/s11214-023-00972-0

Mazarico E, Neumann GA, Rowlands DD, Smith DE (2010) Geodetic constraints from multi-beam laser altimeter crossovers. J Geodesy 84(6):343–354. https://doi.org/10.1007/s00190-010-0379-1

McEwen A, et al (2019) The IO volcano observer (IVO): follow the heat. In Lunar and planetary science conference, vol. 2132

McKinnon WB, Kirk RL (2014) Triton. Encycl Solar Syst. https://doi.org/10.1016/B978-0-12-415845-0.00040-2

Michel P et al (2022) The ESA hera mission: Detailed characterization of the DART impact outcome and of the binary asteroid (65803) didymos. Planet Sci J 3(7):160. https://doi.org/10.3847/psj/ac6f52

Naidu S et al (2020) Radar observations and a physical model of binary near-Earth asteroid 65803 Didymos, target of the DART mission. Icarus 348:113777. https://doi.org/10.1016/j.icarus.2020.113777

National Academies of sciences, Engineering and medicine (2022) Origins, worlds, and life: a decadal strategy for planetary science and astrobiology 2023–2032. The National Academies Press, Washington

Rambaux N, Williams JG (2010) The Moon's physical librations and determination of their free modes. Celest Mech Dynam Astron 109(1):85–100. https://doi.org/10.1007/s10569-010-9314-2

Rambaux et al (2011) Librational response of Europe, Ganymede, and Callisto with an ocean for a non-keplerian orbit. A&A 527:A118. https://doi.org/10.1051/0004-6361/201015304

Richardson DC et al (2022) Predictions for the dynamical states of the Didymos system before and after the planned DART impact. Planet Sci J 3(7):157. https://doi.org/10.3847/psj/ac76c9

Rivkin AS, Cheng AF (2023) Planetary defense with the double asteroid redirection test (DART) mission and prospects. Nat Commun. https://doi.org/10.1038/s41467-022-35561-2

Rosat S, Rosenblatt P, Trinh A, Dehant V (2008) Mars and mercury rotation variations from altimetry crossover data: feasibility study. J Geophys Res. https://doi.org/10.1029/2008je003233

Rymer AM et al (2021) Neptune Odyssey: a flagship concept for the exploration of the neptune-triton system. 2(5):184. https://doi.org/10.3847/psj/abf654

Sabadini R, Vermeersen B (2004) Multi-layer models. In: Sabadini R (ed) Global dynamics of the earth. Springer, Dordrecht, pp 45–97

Sagnac G (1913) L'éther lumineux démontré par l'effet du vent relatif d'éther dans un interféromètre en rotation uniforme. Comptes Rendus 157:708–710

Stark A et al (2015) First MESSENGER orbital observations of mercury's librations. Geophys Res Lett 42(19):7881–7889. https://doi.org/10.1002/2015gl065152

Steinbrügge G, Stark A, Hussmann H, Sohl F, Oberst J (2015) Measuring tidal deformations by laser altimetry. a performance model for the ganymede laser altimeter. Planet Space Sci 117:184–191. https://doi.org/10.1016/j.pss.2015.06.013

Steinbrügge G, Padovan S, Hussmann H, Steinke T, Stark A, Oberst J (2018) Viscoelastic tides of mercury and the determination of its inner core size. J Geophys Res Planets 123(10):2760–2772. https://doi.org/10.1029/2018je005569

Tajeddine R, Rambaux N, Lainey V, Charnoz S, Richard A, Rivoldini A, Noyelles B (2014) Constraints on mimas' interior from cassini ISS libration measurements. Science 346(6207):322–324. https://doi.org/10.1126/science.1255299

The PIONEERS consortium (2019) Pioneers website. https://h2020-pioneers.eu/index.php. Accessed on 20 Oct 2023

Thomas P (2000) The shape of triton from limb profiles. Icarus 148(2):587–588. https://doi.org/10.1006/icar.2000.6511

Thomas P et al (2016) Enceladus's measured physical libration requires a global subsurface ocean. Icarus 264:37–47. https://doi.org/10.1016/j.icarus.2015.08.037

Thomas CA et al (2023) Orbital period change of dimorphos due to the DART kinetic impact. Nature 616(7957):448–451. https://doi.org/10.1038/s41586-023-05805-2

Tyler RH (2009) Ocean tides heat enceladus. Geophys Res Lett. https://doi.org/10.1029/2009gl038300

Van Hoolst T (2015) Rotation of the terrestrial planets. Treat Geophys 10:121–151

Van Hoolst T, Baland R-M, Trinh A (2013) On the librations and tides of large icy satellites. Icarus 226(1):299–315. https://doi.org/10.1016/j.icarus.2013.05.036

Van Hoolst T, Baland R-M, Trinh A (2016) The diurnal libration and interior structure of Enceladus. Icarus 277:311–318. https://doi.org/10.1016/j.icarus.2016.05.025

Van Hoolst T, Baland R-M, Trinh A, Yseboodt M, Nimmo F (2020) The librations, tides, and interior structure of Io. J Geophys Res Planets. https://doi.org/10.1029/2020je006473

Wielandt E (2012) Seismic sensors and their calibration. New Manual Seismol Observ Pract 2. https://doi.org/10.2312/GFZ.NMSOP-2_CH5

Yoder CF, Konopliv AS, Yuan DN, Standish EM, Folkner WM (2003) Fluid core size of mars from detection of the solar tide. Science 300(5617):299–303. https://doi.org/10.1126/science.1079645

Yseboodt et al (2013) Influence of an inner core on the long-period forced librations of Mercury. Icarus 226(1):41–51. https://doi.org/10.1016/j.icarus.2013.05.011

Publisher's Note